

Parameter Estimation Based Real-Time Metrology for Exposure Controlled Projection Lithography

Xiayun Zhao, David W. Rosen*

George W. Woodruff School of Mechanical Engineering
Georgia Institute of Technology
Atlanta, Georgia, 30332

*Corresponding author. Tel.: +1 404 894 9668 Email: david.rosen@me.gatech.edu

REVIEWED

Abstract

Exposure Controlled Projection Lithography (ECPL) is a layerless mask-projection stereolithography process, in which parts are fabricated from photopolymers on a stationary transparent substrate. To enable advanced closed-loop control for ECPL, an in-situ interferometric curing monitoring (ICM) system has been developed to infer the output of cured height. However, the existing ICM method based on an implicit model and rough phase counting is not fast and accurate enough. This paper reports on a new ICM method to address the modeling and algorithms issues confronted by the current ICM method. The new ICM model includes two sub-models: a sensor model of instantaneous frequency based on interference optics and a calibration model. To solve the models, a moving horizon exponentially weighted online parameter estimation algorithm and numerical integration are adopted. As a preliminary validation, offline analysis of interferograms acquired in an ECPL curing experiment is presented. The agreement between ICM estimated cured height and ex-situ microscope measurement indicates that the overall scheme of the new ICM measurement method with a well-established model, evolutionary estimation and incremental accumulation, is promising as a real-time metrology system for ECPL. The new ICM method is also shown to be able to measure multiple voxel heights consistently and simultaneously, which is desired in global measurement and control of ECPL.

1. Introduction and Motivation

1.1 ECPL System Overview

The Digital Micromirror Device (DMD) based Exposure Controlled Projection Lithography (ECPL) system falls into the category of non-stacking mask projection stereolithography apparatus. It has promising applications in fabrication of microfluidics and micro optics components for biomedical devices. Differing from a conventional laser scan stereolithography process, ECPL cures a 3D part by projecting patterned ultraviolet (UV) radiation from beneath through a stationary and transparent substrate. The UV light beam is shaped by a timed sequence of DMD bitmaps, which display time-varying exposure patterns. As illustrated in Figure 1, the ECPL process consists of the following basic steps - resin chamber setup, photopolymerizable material preparation, UV exposure curing, post-developing and washing. As one measure of process resolution, the magnification of the projected DMD on the resin chamber is 0.55 so a projected micro-mirror has a size of approximately 6.8 μm .

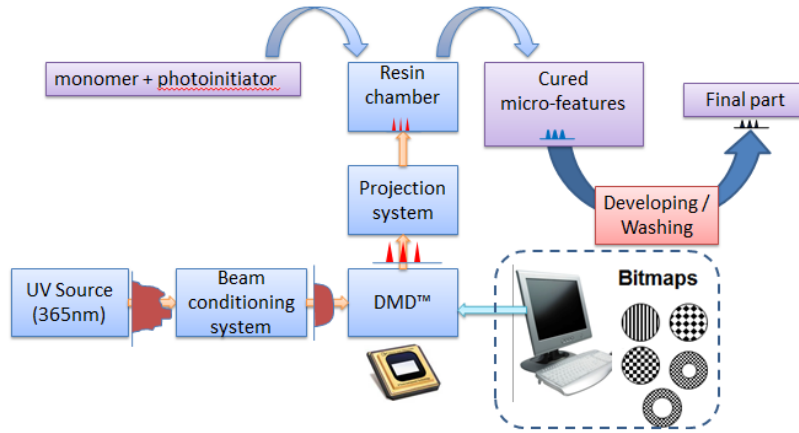


Figure 1: Exposure Controlled Projection Lithography Process Overview [1]

1.2 ICM System Overview

To identify the inherent variations of cured height with on-going exposure and provide reference to identify fabrication errors induced by post-cure processes such as washing and final part measurement, Jariwala (2013) [1] designed an in-situ interferometric curing monitor (ICM) system for the ECPL process. The ICM system, as seen in Figure 2, is based on a Mach-Zehnder interferometer [2]. A coherent laser is directed, through a beam expander, moveable iris, and beam splitter, at the resin chamber. Light reflecting off the interface surfaces of the resin chamber reflects through the beam splitter and into the camera. Due to the optical path differences between the light beams reflected from different interface surfaces, an interference pattern is observed by the camera.

The laser source is a small, low-power, 532 nm wavelength laser diode, which provides the coherent laser light required for interferometry. The beam expander expands the narrow beam produced by the laser source such that the light output could cover the entire curing area in the resin chamber and the camera can capture a full-field interferogram. The movable iris can adjust the size of the incident beam and selectively illuminate a specific location on the curing plane. The beam splitter reflects the laser source downward into the resin chamber while, at the same time, allowing for light coming from the resin chamber to pass through to the camera above. The camera captures the intensity of incoming laser light from the resin chamber, and provides an interference pattern of intensity profile across the illuminated chamber area.

1.3 Motivation

ECPL still has limited process accuracy to become a more capable micro manufacturing method for wider applications. With the development of the in-situ ICM system ([2], [3]), the accuracy plateau of existing open-loop process controls might be changed with a more mature ICM, which will be able to provide real-time measurement output enabling a closed-loop control. Hence, we desire an upgraded ICM system from in-situ monitoring into a real-time metrology system for a synthetic ECPL system with measurement and control systems as envisioned in Figure 3.

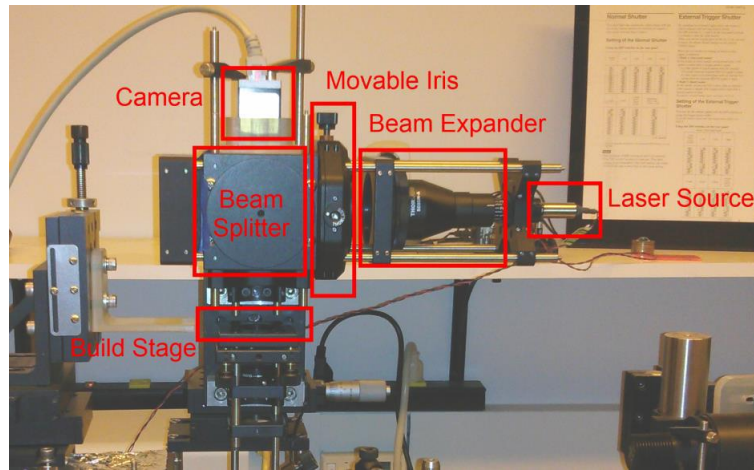


Figure 2: ICM System

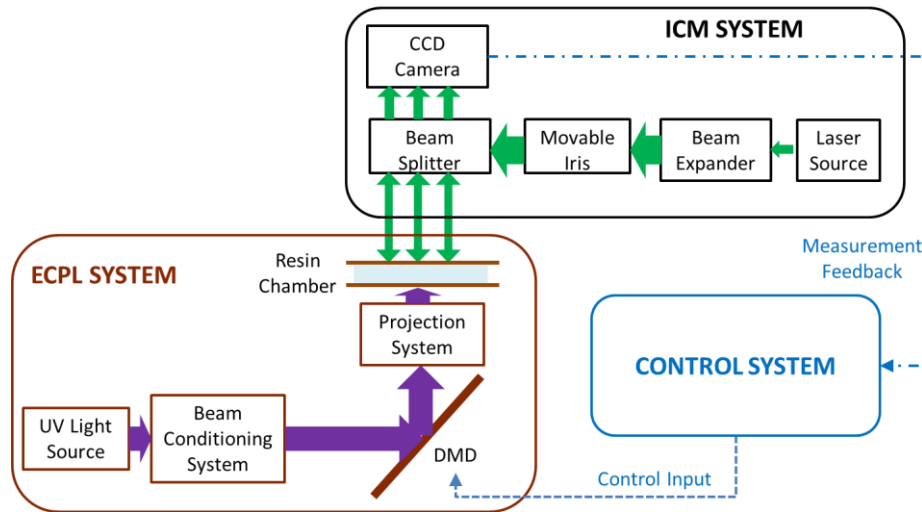


Figure 3: An Integrated ECPL System with Real-time Measurement and Control

2. Issues of Real-time Measurement with ICM System

The current ICM system needs further development in measurement theory and algorithms for interpreting the sensor data in real-time metrology. Various interferometry techniques and applications exist; however, there is no handy solutions to the real-time ICM measurement because:

1) The ICM measurand – photopolymerized part dimensions – involves complex unknown material properties and variations. Hence, a measuring principle model, i.e., an ICM model, is needed in order to interpret the interferogram accurately and to extract the desired measurement variables. The ICM model should consist of two sub-models: interference optics sensor model and calibration model, both of which decide the unique issues and inherent challenges in real-time measurement with the ICM system.

2) Many existent techniques of interferogram signal processing deal with spatial interferograms instead of temporal interferograms as in the ECPL case. Techniques for phase measurement can be split into two basic categories: electronic method which utilizes hardware of phase modulator, and analytical method of fringe pattern analysis such as Fourier transform

which commonly adopts a phase shifter in one beam [4]. A different approach, based on a 1D unwrapping along the time axis rather than on a 2D spatial unwrapping, is needed for an important subclass of interferometry applications [5].

3) Existing literature provides two approaches of temporal phase measurement: temporal phase shifting with a carrier modulation and Fourier analysis of time-dependent intensity signals [6, 7]. However, the ICM is not configured to be able to add a temporal carrier in the coherent light to modulate the intensity. If the latter method is used, it is possible to measure the phase without introducing a carrier, but the sign of the displacement cannot be deduced.

4) Even though there is some research on the temporal phase unwrapping topic, real-time measurement is rarely addressed and most of the algorithms are for posterior offline analysis. Gao, Huyen (2009) [8] proposed a parallel algorithm with a special GPU (Graphics Processing Unit) card and achieved only 4 fps for 256×256 digital fringe patterns real-time windowed Fourier filtering. Real-time measurement demands both hardware and software to sufficiently be fast and precise [9].

5) Some literature even requires the measured object to have special characteristics to implement its approach. For instance, Huntley and Saldner (1993) [5] assumed implicitly that the deformation rate was sufficiently low for negligible phase change to occur over the time scale required to digitize one set of phase-stepped images. This does not apply to ECPL process measurement which is fast and cannot use a four-step interferometer where four intensity values at a phase increment of $\pi/2$ are required.

The existing ICM system could potentially provide a real-time metrology to aid advanced controller design. It has already provided insights into the real-time photopolymerization process, interferograms of which demonstrated vividly the stages of incubation period, exposure curing and dark reaction in ECPL process. However, Jariwala [1] used ICM for process monitoring process only, because it was only a qualitative and non-direct visualization of the curing process. Jones [10] mainly employed simple data smoothing and maxima estimation codes to quantitatively count the phase angle in real-time but not fast or complete enough for a reliable and comprehensive real-time measurement.

Both existing approaches of using ICM to obtain information of cured heights are limited in the following aspects [11].

1) An interference optics model [1-3, 10, 12] as shown in Eq. (1), which models a linear relationship of phase angle ϕ and refractive index change Δn . However, to obtain the cured height, an empirical logarithmic curve is used to fit the cured height from phase shift ϕ as Eq. (2) [10]. The two equations together imply a logarithmic relation between the two compounding variables of overall resin refractive index change Δn and cured height Z . This logarithmic relationship needs justification otherwise an improved or modified model will be required.

$$\text{Phase Angle } \phi = 2\pi \cdot \left(\frac{2 \cdot \Delta n \cdot t}{\lambda} \right) \quad (1)$$

$$\text{Cured Height } Z = 78.96 \cdot \ln(\phi) - 259 \quad (2)$$

where Δn is the change in overall refractive index, t is the fixed chamber height, λ is the coherent laser wavelength.

2) The calibration by curve fitting an empirical model of intensity oscillation phase angle and cured height lacks a firm basis in physical phenomena and is not amenable in practice due to batch-by-batch and operator-by-operator variations.

3) The simple method of phase angle counting of extrema is problematic in both accuracy and real-time implementation. By identifying a half-cycle from peak and valley extrema, the method has limited resolution fixed at π , and phase angle less than π is prone to interpolation errors, which might be significant especially in the case of non-constant periods and amplitudes. The unknown process variations and irregular oscillation patterns also makes it difficult to predict the next peak or valley.

4) Considering the intensity dynamics of a single point could be highly biased, because it is not necessarily representative or comprehensive across the entire part. Accuracy is limited by the unwanted irradiance variations arising from nonuniform light reflection or transmission by the test object spatially.

As summarized in Table 1, ICM still confronts some modeling and methodology issues to be completely eligible as real-time measurement of cured heights to provide output feedback for an advanced controller. This paper will present a proposed newly developed method of ICM measurement model and algorithm to solve the issues.

Table 1. Research Gaps in ICM real-time measurement

ICM Methods	Sensor Model	Calibration Model	Measurement Mode (Online Vs. Offline)	Data Analysis Method	Measured Area
Existing	Implicit model confounding two critical variables: the changes in effective refractive index and cured height.	Arbitrarily use logarithmic curve fitting of Experimental data of cured height Vs. phase angle. Lack physics justification, and reproducibility.	Mainly Offline. Slow and Inaccurate online measurement, Unready in Real-time Execution	Count phase angle by peak-valley extremas in an increment of pi. Inaccurate, and impractical in real-time implementation.	Single point
Proposed	Elaborated optics model with explicit parameters and variables.	An established mathematical method to calculate cured height from the sensor model with more confidence.	Online and Mature Real-time	Extract the phase angle information robustly by a fourier model. Online parameter estimation, and numerical integration.	Multiple point, Full field

3. ICM Model

The ICM system aims to utilize the principles of interferometry to measure the dimensions, particularly the height at the current research stage, of the part cured in the resin chamber. In future work, it could be extended to 2D and 3D measurement. The sequential acquisition of a large number of interferograms and their postprocessing facilitates the recovery of the phase distribution, so that the whole-field dynamic displacement field can be determined [13]. In this framework, the phase distribution is commonly recovered using a temporal phase shifting algorithm, and the unwrapping is performed as a function of time. Transform-based or reference-based approaches could be used to retrieve optical phase distributions coded in the temporal intensity [6, 14, 15]. Hence, signal processing of the pixel intensity time series could recover the cured height, based on a well-established ICM model which consists of two sub-models. One sub-model is the sensor model of interference optics that explains the intensity dynamics in the interferogram sequence. The other sub-model is the calibration model that calculates the measured variable of cured height from ex-situ microscope measurement and estimated parameters in the sensor model.

3.1 ICM Sensor Model

For ICM, the camera records frames of the spatial interferogram produced by the optical path length differences of the light reflecting from the interface surfaces thru the resin chamber. A temporal intensity oscillation in the interferogram sequence is evident for pixels across the curing area, because the optical path length of the light reflecting from the top and bottom surfaces of the cured part changes with time as the photopolymerized resin cures in the chamber.

The resultant temporal interference pattern presents a time series of intensity for each pixel across the chamber. The curing process causes the resin refractive index to change from n_l to n_s as it crosslinks from liquid into solid. Meanwhile, it changes the height of liquid resin and solid resin in the chamber. Both changes in medium refractive index and height lead to a change in optical path length thus in the interferogram phase.

3.1.1 Multi-beam interference optics

Firstly, a prototype sensor model based on multiple beams interference optics is built for ICM. An example case of the interference of five optical waves is illustrated in Figure 4, where it is assumed that the waves interfere above any curing point in space after reflection and refraction in the resin chamber. It is noted that due to the special configuration of perpendicular incidence in ICM, the waves are assumed to be linearly polarized at the same plane and travelling in the vertical direction. Meanwhile, other possible beams are omitted because chances are these beams have been attenuated greatly and become insignificant after multiple reflections, scattering and absorption.

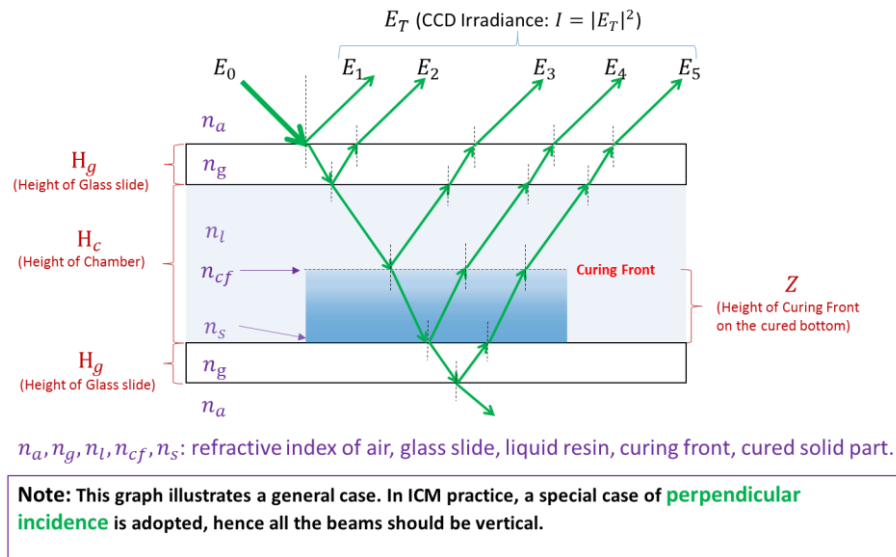


Figure 4. Multi-beam Interference Optics Model for ICM

Furthermore, a key simplifying factor in the analysis of the interference optics model in Figure 4 is the use of a virtual interface; that is, curing front to extract values of both the refractive index and growth rate of a film [16]. It has been shown that multiple-layer film is mathematically the same as a single layer on an “effective interface”, which is the case for compound semiconductor films where both chemical composition and growth rate need to be determined [16]. The concept of single virtual interface could also be applied in the ECPL resin curing process with the same assumption that each thin cured layer is homogeneous and isotropic with fixed refractive index and growth rate in the plane normal to the incidence direction.

The phenomenon of interference occurs when multiple waves overlap. In Figure 4, mathematically the vector addition of the wave components in Eq. (3) results in a total wave of Eq. (4).

$$E_n = A_n e^{i\phi_n}, n = 1, 2, \dots, 5 \quad (3)$$

where, A_n is the real positive amplitude, ϕ_n is the phase angle of each wave.

$$E_T = \sum_{n=1}^5 E_n = \sum_{n=1}^5 A_n e^{i\phi_n} \quad (4)$$

When the field is observed by a CCD camera, the result is the average of the field energy by area unit during the integration time of the camera, that is, the irradiance I [17], which is proportional to the squared module of the amplitude as shown in Eq. (5).

$$I = |E_T|^2 = \left| \sum_{n=1}^5 A_n e^{i\phi_n} \right|^2 = \sum_{n=1}^5 |A_n|^2 + 2 \sum_{j=1}^5 \sum_{\substack{k=1 \\ k \neq j}}^5 A_j A_k \cos(\delta_{jk}) \quad (5)$$

where, $\delta_{jk} = \phi_j - \phi_k$, is the relative phase difference between the component of each wave (for simplicity, the temporal and spatial dependencies have been omitted).

The phase differences δ_{jk} in Eq. (5) are caused by optical path length differences between each set of two wave components. The stationary items such as δ_{21} stem from beams such as E_1 and E_2 , which have constant path length difference - a product of the glass slide height and refractive index in the case of δ_{21} . Hence, the term of δ_{21} in Eq. (5) will contribute to the average, i.e., DC (direct current), term in the detected intensity signal. Only the changing optical path length will contribute to the detected cycling of interferogram intensity. The oscillation, i.e., AC (alternative current), terms come from the beams E_3 , E_4 and E_5 , whose optical path are affected by the curing block in the chamber.

The ICM aims to measure the ECPL process dynamics, thus the oscillation of intensity signal is of interest. It is worth noting that the AC terms in the intensity signal convey information about the optical path length difference (OPLD) coupling both varying height and refractive index in the curing block. As noted in the virtual interface in the optics model, the curing front is an imaginary interface between the uncured liquid resin and curing part, which is defined as the whole curing block that might consist of intermediate phases between liquid and solid depending on the curing degree – portion of cross linked monomers [18]. Thus the cured height is defined as the height of the curing front relative to the cured solid bottom. As shown in Eqn. (6), one can use the integral form of the cured height and refractive index to calculate the OPLD between the beams E_3 and E_4 thru the curing part with a curing front at height z . The vertical distribution of refractive index is assumed continuous as the curing proceeds, and thus according to the mean value theorem of integration, there exists an intermediate value n_m between n_s and n_{cf} such that the OPLD is a product of the height z and n_m .

$$OPLD_{E_4-E_3} = \int_0^z n(x) dx = n_m z, \quad \text{where } n(0) = n_s, n(z) = n_{cf} \quad (6)$$

where, n_s and n_{cf} are the refractive indices of cured solid bottom and curing front respectively, n_m is the mean, i.e., effective refractive index of the curing part. All are assumed to be constant.

According to the model in Figure 4 and Eqn. (5) - (6), the phase difference components are analyzed as shown in Table 2. The red items highlight time-varying items which induce the oscillations in intensity captured by the CCD camera in ICM.

Table 2. Phase Component Analysis of the Multi-beam Interference Optics Model in ICM

No.	Phase Difference	Source Beams	Role
1	$\delta_{21} = \frac{4\pi}{\lambda} n_g H_g$	E_1, E_2	Constant DC term
2	$\delta_{31} = -\frac{4\pi}{\lambda} n_l Z + \frac{4\pi}{\lambda} n_l H_c + \delta_{21}$	E_1, E_3	Oscillating AC term
3	$\delta_{41} = \frac{4\pi}{\lambda} (n_m - n_l) Z + \frac{4\pi}{\lambda} n_l H_c + \delta_{21}$	E_1, E_4	Oscillating AC term
4	$\delta_{51} = \frac{4\pi}{\lambda} (n_m - n_l) Z + \frac{4\pi}{\lambda} n_l H_c + 2\delta_{21}$	E_1, E_5	Oscillating AC term
5	$\delta_{32} = -\frac{4\pi}{\lambda} n_l Z + \frac{4\pi}{\lambda} n_l H_c$	E_2, E_3	Oscillating AC term
6	$\delta_{42} = \frac{4\pi}{\lambda} (n_m - n_l) Z + \frac{4\pi}{\lambda} n_l H_c$	E_2, E_4	Oscillating AC term
7	$\delta_{52} = \frac{4\pi}{\lambda} (n_m - n_l) Z + \frac{4\pi}{\lambda} n_l H_c + \delta_{21}$	E_2, E_5	Oscillating AC term
8	$\delta_{43} = \frac{4\pi}{\lambda} n_m Z$	E_3, E_4	Oscillating AC term
9	$\delta_{53} = \frac{4\pi}{\lambda} n_m Z + \delta_{21}$	E_3, E_5	Oscillating AC term
10	$\delta_{54} = \frac{4\pi}{\lambda} n_g H_g = \delta_{21}$	E_4, E_5	Constant DC term

3.1.2 Instantaneous Frequency Analysis

The phase components listed in Table 2 reveal that the oscillating phases are all attributed to the cured height Z , the change rate of which is the curing velocity. Because the nonlinear ECPL process is known to exhibit non-constant curing velocity, the ICM signal in Eq.(5) has frequency content that changes over time. The instantaneous frequency (IF) represents one of the most important parameters in the analysis of such signals with time-varying frequency [19]. Despite the possibility that light intensity and material properties (e.g. n_l, n_s, n_{cf}, n_m) are subject to change with time during the process, for a short duration, these factors may be assumed to be constant. With the assumption that all the process parameters are momentarily invariant, the only varying factor is the cured height, and thus the IF, defined as the time differential of phase, is only associated with the curing velocity \dot{Z} . As shown in Table 3, the IF components based on the phase components in Table 2 are analyzed.

Table 3. Instantaneous Frequency of the Multi-beam Interference Optics Model in ICM

Instantaneous Frequency (Hz)	Corresponding Phase	Estimated Value (Hz)
$f_0 = 0$	δ_{21}, δ_{54}	0
$f_1 = \frac{2}{\lambda} n_l \dot{Z}$	δ_{31}, δ_{32}	31.5
$f_2 = \frac{2}{\lambda} n_m \dot{Z}$	δ_{43}, δ_{53}	32.1
$f = \frac{2(n_m - n_l) \cdot \dot{Z}}{\lambda}$	$\delta_{41}, \delta_{51}, \delta_{42}, \delta_{52},$	0.6

A rough estimation of the IF values is performed using the experimental data obtained by Jones, Jariwala (2014) [10], who cured a 51.5 μm part in 9 seconds with the same material composition. Hence, the average curing velocity \dot{Z} is about 5.7 ($\mu\text{m}/\text{s}$). The interferograms intensity signal is about 0.6 Hz, which is obviously the lowest non-zero frequency component f in Table 3. Since the refractive index of resin n_l is 1.4723 [12], one could back-calculate $(n_m - n_l) = 0.0279$ by plugging the average \dot{Z} of 5.7 into $f = \frac{2(n_m - n_l)(5.7)}{0.532} = 0.6$ Hz. Hence, the mean effective refractive index n_m was estimated to be 1.5002. Furthermore, the other two frequency components could be estimated as below.

$$f_1 = \frac{2}{\lambda} n_l \dot{Z} \cong \frac{2}{0.532} (1.4732)(5.7) = 31.5 \text{ Hz}$$

$$f_2 = \frac{2}{\lambda} n_m \dot{Z} \cong \frac{2}{0.532} (1.5002)(5.7) = 32.1 \text{ Hz}$$

The IF analysis above concludes that three non-zero instantaneous frequencies exist in the ICM intensity signal. However, the actually observed ICM intensity signal frequency is low about 0.6 Hz. Two possible reasons could explain that only the low frequency component f is detected in the captured signal. Firstly, f_1 and f_2 are about 30Hz and cannot be detected by the CCD camera with a sampling frequency of 30Hz, which could detect up to 15 Hz signal according to the Nyquist theorem. Secondly, both f_1 and f_2 involve the beam wave E_3 , which is modeled to reflect from the vague virtual curing front that has a refractive index close to the liquid resin and thus has very small amplitude due to a weak reflectivity.

3.1.3 Established ICM Sensor Model

As a summary, the ICM directly-measured intensity I_M is modeled as a sum of the reference and all the low instantaneous frequency f components in the multi-beam interference optics model. Note that all the cosine terms with frequency f but different amplitudes and phase offset can add up to a single cosine wave, which still preserves the same frequency but possesses different phase offset and amplitude. The multi-beam interference optics model in Eq.(5) ends up with a lumped single-frequency cosine formula, which resembles what has been observed from the ICM interferogram signal.

Finally, the ICM sensor model is derived as shown in Eq. (7) and (8).

$$I_M = I_0 + I_1 \cos(\delta + \varphi) = I_0 + I_1 \cos\left(\frac{4\pi(n_m - n_l)}{\lambda} \cdot Z + \varphi\right) \quad (7)$$

$$\omega = 2\pi f = \frac{d(\delta + \varphi)}{dt} = \frac{d\delta}{dt} = \frac{4\pi(n_m - n_l)}{\lambda} \cdot \frac{dZ}{dt} \quad (8)$$

where, I_M is the directly measured intensity by CCD camera; I_0 is the overall average intensity; I_1 is the superposed intensity of all the interference beams with the same instantaneous frequency f ; δ is the time-varying phase component in the intensity model; φ is the static superposed phase offset of all the interference beams with the same frequency; f , ω are the instantaneous frequency and instantaneous angular frequency, respectively; λ is the laser wavelength $0.532\mu\text{m}$, n_m and n_l are mean cured and liquid part refractive index.

3.2 ICM Calibration Model

With the established ICM sensor model that illustrates the intensity signal, we desire to further infer the measurand – cured height from it. Hence, the other ICM sub-model, i.e., calibration model, is required to calculate the cured height from the estimated parameters of instantaneous frequency in the sensor model along with the calibrated parameters of refractive index in the ex-situ measurements.

By rewriting Eq.(8), a differential form of the cured height is derived in Eq.(9).

$$\frac{dZ}{dt} = \frac{\omega\lambda}{4\pi(n_m - n_l)} = \frac{f}{2(n_m - n_l)} \quad (9)$$

To evaluate the cured height from the differential form in Eq.(9), a numerical integration approach using Euler's Method is proposed as below in Eq.(10), which forms the ICM calibration model.

$$Z = \sum_i \frac{\lambda T_i}{4\pi(n_m - n_l)} \cdot \omega_i = \sum_i \frac{\lambda T_i}{2(n_m - n_l)} \cdot f_i \quad (10)$$

where T_i is the time step of integration, f_i (or ω_i) is the instantaneous (angular) frequency in the i^{th} run of parameter estimation. The refractive index term $(n_m - n_l)$ requires calibration with ex-situ microscope measurements of cured height.

Eqns (9) and (10) have two uses. First, one of them can be used to estimate the refractive index term $(n_m - n_l)$, as explained in Section 3.1.2 where $(n_m - n_l)$ was computed using Eq.(9) with a rough estimation of the average curing velocity $\frac{dZ}{dt}$ and observed average frequency f . However this approach may not be as accurate as a more practical calibration procedure adopting Eq.(10). Ideally, a standard calibration procedure should adopt the calibration model in Eqn.(10), and plug in the ex-situ microscope measured cured height, Z , to find out the value of $(n_m - n_l)$, which, in turn, could be used for succeeding measurements to compute cured height in Eqn.(10). This approach will be investigated in future work.

4. Parameter Estimation for ICM Model

In the ICM model, the cured height of a voxel is coded in the temporal intensity dynamics observed in the corresponding camera pixel. It is discovered that adjacent voxels, which are

expected to have close if not identical cured heights, share similar phase angles across the curing area. Hence, Fourier analysis along the time-axis is one candidate method to evaluate the phase map [6], but the Fourier transform based analysis is efficient only when the frequency content of the analyzed signal does not change over time. In the ICM application, one deal with signals where the cured height information is conveyed within time-variations of the signal's instantaneous frequency that corresponds to the curing velocity. Hence, a method of time-frequency analysis [19] is needed to solve the ICM model, which requires estimation of the unknown parameter of instantaneous frequency f or ω to calculate the cured height.

4.1 Curve Fitting with One-term Fourier Model

A curve fitting method is adopted to minimize the square errors between the sensor model prediction and measurement. Because there is only one outstanding frequency in the ICM sensor model, the method of 'fourier1' - a Fourier series model with only one frequency item as shown in Eq. (11), is used in the curve fitting to estimate the instantaneous frequency locally.

$$y = f(x) = a_0 + a_1 \cdot \cos(px) + b_1 \cdot \sin(px) \quad (11)$$

It could be written into the trigonometric form as shown in Eq. (12).

$$y = f(x) = a_0 + \sqrt{a_1^2 + b_1^2} \cdot \cos(px + \theta), \quad (12)$$

$$\text{where } \theta = \tan^{-1}\left(-\frac{b_1}{a_1}\right)$$

Note that in Eq. (11) and (12) the sampling index x and the time t is converted by $t = \frac{x}{f_s} = \frac{x}{30}$ (s), because the camera acquisition frame rate is $f_s=30$ fps.

The one-term Fourier model is written into a form as shown in Eq. (13), which is mapped to the ICM sensor model, and used to estimate the instantaneous angular frequency ω .

$$y = f(t) = a_0 + \sqrt{a_1^2 + b_1^2} \cdot \cos(\omega t + \theta), \quad (13)$$

$$\text{with } \omega = f_s \cdot p, \theta = \tan^{-1}\left(-\frac{b_1}{a_1}\right)$$

where f_s is the camera acquisition frequency ($f_s = 30$ fps in this case), p is the estimated "frequency" in the Fourier model in Eqn. (12).

4.2 Online Parameter Estimation with Moving Horizon Exponentially Weighted Fitting

The conventional least squares method that assumes constant parameters over the entire curing period may not work in this case [20], because the assumption of static parameters is only valid in a short time. During the entire curing period, the growth velocity of the cured part tends to change with the temperature, composition, and microstructure. An in situ sensor must be able to deal with a time-varying process if feedback control is to be used. In on-line parameter estimation, a model is fitted optimally to the past and present process measurements while the process is in operation [21]. For the ICM application, parameter estimation via on-line

optimization can be performed by solving online a minimization problem such as sum of squared errors in the abovementioned ‘Fourier 1’ curve fitting. This parameter estimator can have an increasing (with time) or constant horizon. An estimator with an increasing horizon has been referred to as batch estimator and one with constant horizon as moving horizon estimator. A solution to the ICM model with varying instantaneous frequency is to fit the parameters over a short window of data, i.e., a moving horizon.

Exponential weighting is typically used in a recursive update procedure for parameter estimation. Figure 5 compares curve fitting without and with weights. The left graph displays an unweighted fitting which fits a much shorter length of latest data and could not estimate the current frequency as well as the weighted fitting did in the right graph. This demonstrates the necessity of applying exponential weights to fit the Fourier model for the most recent set of data, which is critical in estimating the latest instantaneous frequency.

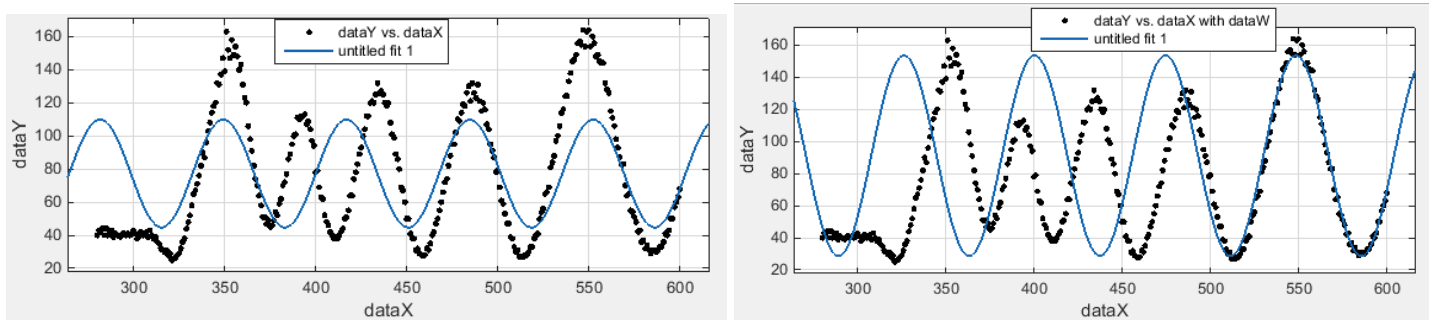


Figure 5. The need for exponentially weighted curve fitting to improve the curve fitting for most recent data (Left: unweighted fitting; Right: exponential weighted fitting)

Conclusively, a windowed exponentially weighted curve fitting with moving horizon, or simply “rolling fit”, is developed for ICM parameter estimation. With the one-term Fourier model in Eq. (13), and given a sequence of measurements in a window size m starting from $j - m + 1$ up to j along with exponential decay half life, the parameters in this window can be estimated by solving the following minimization problem in Eq. (14). Note that “half life” means the width decaying weight to one half, and it is related to the exponential decay constant τ by a factor of $\ln(2)$.

$$\min \sum_{l=j-m+1}^j e^{-\frac{j-l}{\tau}} (y_{l_{meas}} - y_{l_{fitted}})^2 \quad (14)$$

where $\tau = half_life / \ln(2)$, and $y_{l_{meas}}, y_{l_{fitted}}$ is the l^{th} measured and fitted data respectively in the curve fitting with one-term Fourier model.

When new measurement data are acquired, the window is shifted to include these new data and at the same time part of the old data is discarded using a suitable forgetting factor – exponential weights in this case. The training data set is used to estimate the sensor model parameters, and succeeding (or test set) data are used to validate the accuracy of the parameters. In other words, the estimated parameters in the current run of rolling fit is applied to a rolling prediction for upcoming measurement data, in order to verify the estimation accuracy and prediction capability, which is critical for real-time measurement and control.

4.3 Effects of Window Length in the Estimator

The ICM model assumption will hold better for smaller time steps, which will be limited by the available computation resources. In this study, the time step of each estimation iteration consists of every 5 sampling frames corresponding to about 1/6 second. Correspondingly, a half life of “5” is chosen for the calculation of exponential weights. In an initial study of an ICM pixel intensity signal, different values of window length are investigated for the rolling fit, and it is found that a window length of “32” yields the lowest mean square errors (MSE) in the rolling prediction as shown in Table 4. One possible explanation is that despite non-constant oscillation cycles, the ICM intensity signal has roughly average periods of about 60 sampling data points and it requires at least half cycle to estimate the period and frequency. But a window length that is too long will slow the algorithm and yield a poor fitting. A window length of “32” turns out to be a reasonable option for real-time computation, good estimation accuracy and prediction performance as well, especially in that the signal peaks and valleys are observed to be fitted much better in the rolling prediction while other window lengths result in serious overshoot (undershoot) at peaks (valleys).

Table 4. Effects of Window Length

Window Length	MSE of Rolling Prediction
Entire	6.54
70	6.56
60	6.32
50	6.10
40	5.95
36	5.61
32	5.57
30	5.71

5. ICM Sensor Method

As a summary, the ICM sensor should sense the local change in the interference pattern, estimate the instantaneous frequency of the interference pattern, and estimate the resulting change in part cure height. This procedure needs to be repeated for each subsequent time period as the part is being fabricated. When part fabrication is completed, an estimate of total cured part height and total interferogram phase angle are produced.

The relationships between the various models presented in Sections 3 and 4, the CCD camera, and the interferograms are shown in Figure 6. As stated, the ICM model includes a sensor model and calibration model, which provide formulated problems for the parameter estimation and cured height algorithms to solve. The algorithm of parameter estimation by moving horizon exponentially weighted “fourier1” curve fitting is developed to estimate the instantaneous frequency f in the sensor model. Note that all the blue symbols in Figure 6 denote frequency items and conversions between the model and algorithms. The calibration model will be used to estimate the key index of refraction difference between solid and liquid resin off-line, then used to compute cured height during on-line operation. The overall scheme of the developed ICM measurement method with evolutionary estimation and incremental accumulation enables a promising real-time implementation.

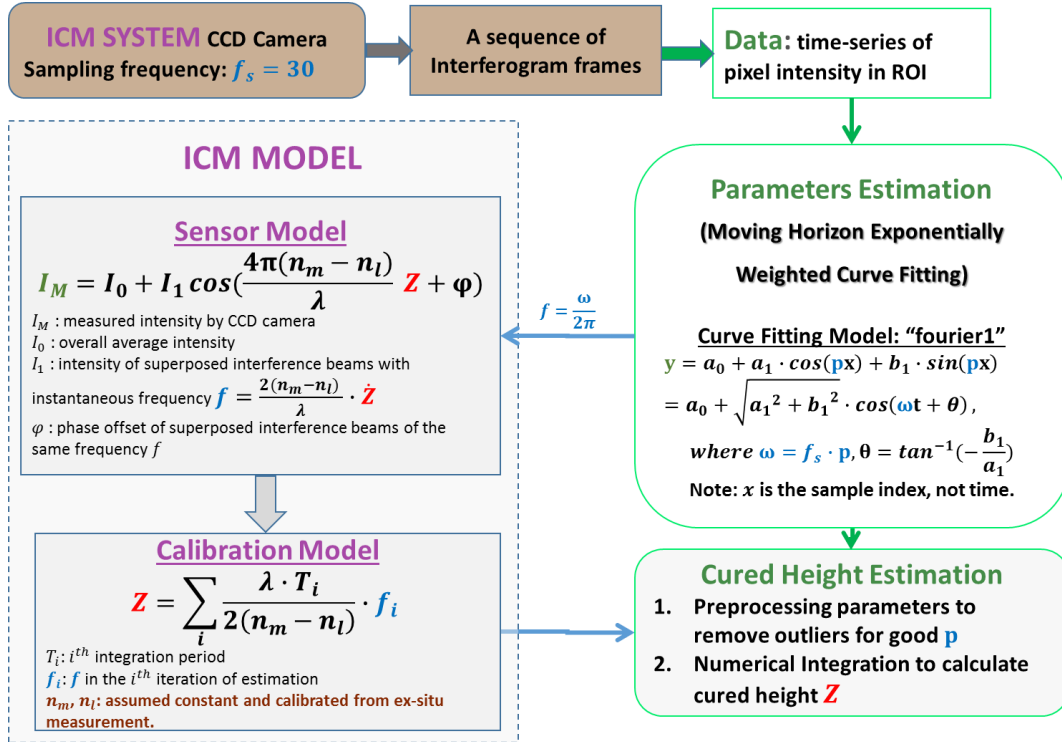


Figure 6. Scheme of ICM Measurement Method: Models and Algorithms

For initial validation of the overall method, a simplified method will be tested in Section 6 for off-line analysis of the curing process described by a set of saved interferograms. For each camera pixel of interest, the curve fitting model “fourier1” is used to compute the local frequencies, f . The data are smoothed to eliminate outlier frequencies in the interferogram dynamics signal. Then, the cured height is computed using Eqn. (10) by numerical integration.

6. Results

To study the feasibility of the ICM method above, an interferogram video recorded by the ICM camera during an experiment of curing a rectangle block was investigated in offline analysis. Measurements are performed for both a single pixel and an area of multiple pixels.

6.1 Calibration of Refractive Index

In this preliminary validation, because we do not have detailed microscope measurements of the part that corresponds to the saved ICM interferogram video, we could not perform the formal calibration with Eq.(10) to get refractive index. Hence, we used the derivative form of the calibration model in Eqn. (9) and an estimation of the cured velocity [10] to calibrate the refractive index difference. As detailed in Section 3.1.2, it was found that $(n_m - n_l) = 0.0279$, which is the value used in this study.

6.2 ICM for Single Pixel

Firstly, a time-series of ICM measured intensity is analyzed offline and a voxel cured height is estimated for the center pixel in the interferogram to validate the proposed ICM measurement method. As shown in Figure 7, the cyan solid line displays a typical time series of pixel intensity in the curing process for one pixel. It is not exactly sinusoidal due to the nonlinear curing process

and stochastic noises including the nonlinear response of camera electronics [7]. The blue data dots in the figure depict the windowed data in the moving horizon of the latest training set, and the red line is correspondingly the fitted curve. The window length is 32 and half life of exponential weights is 5. The fitted curve agrees very well with the current moving horizon.

To further test the estimation accuracy, a simultaneous rolling prediction is performed by applying the estimated parameters in each run of fitting to a test set of 5 succeeding data to predict the test set data values. Figure 8 shows the rolling prediction result for the entire analyzed horizon, where the red predicted data track the actual data with a mean square error (MSE) of 5.6 in greyscale [0, 255], which is acceptable because of various noises in the process and devices. In reality, the fluctuation in measured intensity greyscale is not unusual, which necessitates a filter of measurement error. The rolling prediction MSE on one hand demonstrates that the estimation method of rolling windowed exponentially weighted curving fitting is able to detect the current dynamics and parameters with good accuracy, and more importantly it is shown to be promising for real-time control purposes which may require state prediction.

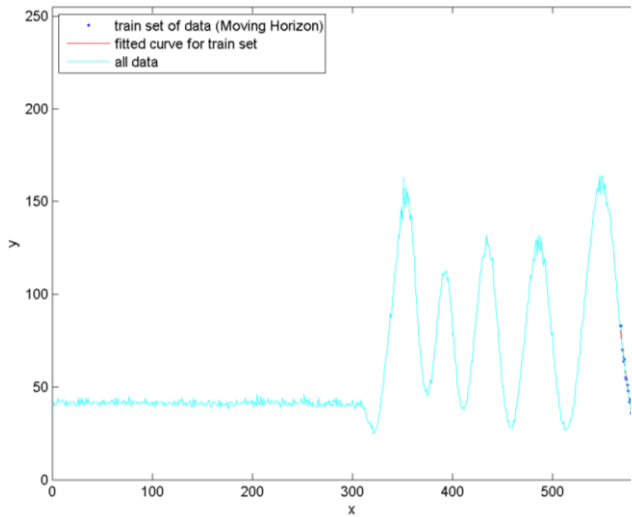


Figure 7. Pixel Intensity Signal and Rolling Fit

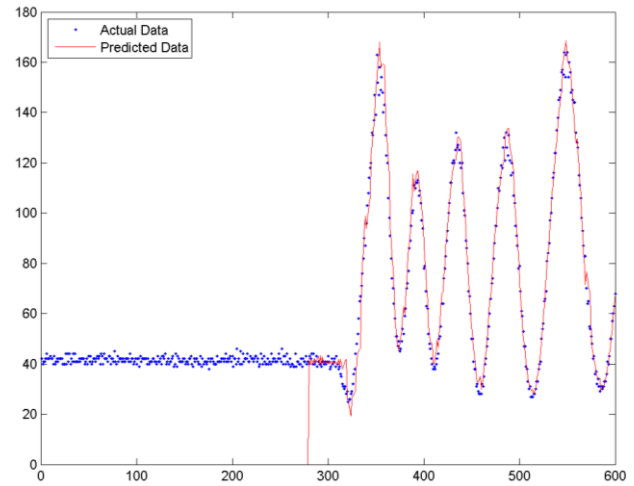


Figure 8. Pixel Intensity Rolling Prediction

Cured height estimation by Eq. (10) for the pixel in the rolling fit and prediction above is shown in Figure 9. The cured height is estimated to be $50.9\mu\text{m}$, while the average measured heights of cured blocks with the same batch of material and same exposure time is $51.5\mu\text{m}$ [10]. The difference may be caused by an incomplete curing window with a small amount of dark curing omitted, and/or by calibration error in the refractive index.

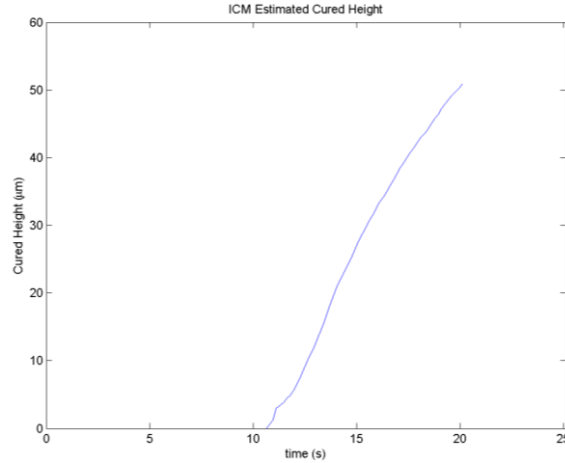


Figure 9. Cured Height of One Pixel

6.3 ICM Measurement for Area of Multiple Pixels

Although good performance was achieved for a single central pixel, it is of greater interest to examine the ICM’s capability in measuring cured heights across a larger area or even full field. The same ICM model, algorithms and refractive index values are applied to a region of 11×11 pixels around the center pixel analyzed above using offline analysis of the same interferogram video. Firstly, the rolling prediction MSE distribution over an area of 121 pixels is shown in Figure 10. The MSE values range from 2.1 to 9.3 with an average of 4.4 in greyscale [0, 255]. With the spatial variation of the curing area and considerable noises, the MSE values are fairly low across the area over time, providing a strong proof that the developed method of moving horizon exponentially weighted “fourier1” curve fitting is viable in online parameter estimation for ICM model.

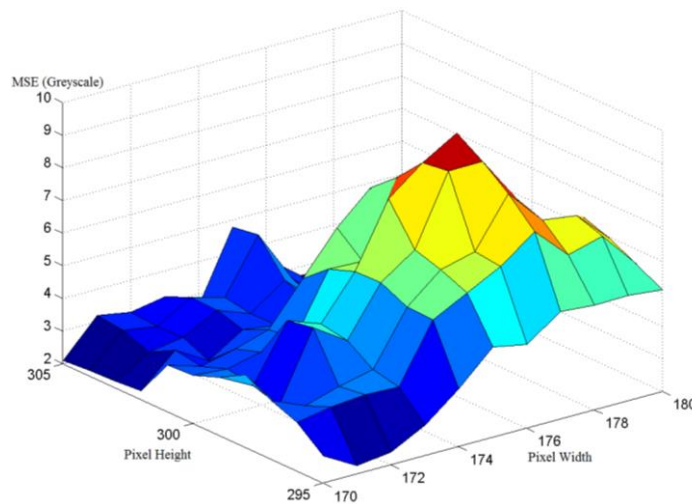


Figure 10. Rolling Prediction MSE for Multiple Pixels

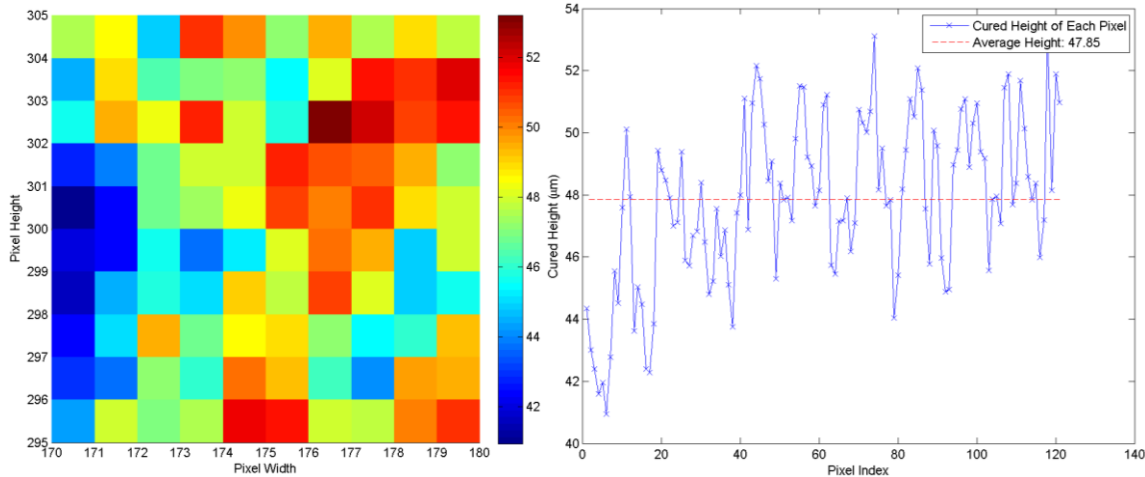


Figure 11. Cured Heights for Area of 11×11 Pixels (Left: 3D Contour View; Right: 1D View)

Figure 11 shows the estimated profile of cured heights across the studied area. The measurements in literature [10] provide only a single value of the topmost area of the cured part, and there was no similar measurement for an area of multiple pixels from the microscope to compare with the ICM evaluation here. However, the range ($40.9 \sim 53.2 \mu\text{m}$) and average ($47.8 \mu\text{m}$) numbers given by our ICM method are reasonably close to the single measurement ($51.5 \mu\text{m}$) from the microscope [10]. The variations of the cured height in Figure 11 might come from the actual spatial roughness and / or noise in the interferograms. If it is for the former reason, the process needs better control to enhance the output accuracy in cured heights all across the curing area. If it is for the latter reason, noise handling and artificial compensation may be used to improve the ICM measurement accuracy. Nevertheless, the encouraging results of multi-pixel cured heights measurement show that the ICM model and method is not restricted to a single point measurement and are promising in achieving the desired full-field measurement capability. Additionally, the off-line analysis of the 121 pixels, including about 80 iterations of parameter estimation and cured height calculation, required less than 5 seconds on a HP laptop with an Intel i7 core microprocessor, which indicates the potential feasibility of real-time sensing for global feedback control.

7. Conclusion

It is common that for all micro manufacturing processes, in order to effectively achieve process control and quality enhancement, improved real-time metrology systems and sensors are needed at the micro level such that true process control can be enabled [22]. This study establishes a real-time metrology for cured heights by processing a time series of pixel intensities in a sequence of interferograms, acquired by an in-situ ICM system. The newly developed ICM method consists of an ICM model and parameter estimation algorithms. It has been demonstrated via a preliminary offline analysis to have the potentiality in real-time and global measurement and control for the ECPL process. Main contribution by the reported work is detailed as below.

1) The multi-beam interference optics model was used to successfully perform an innovative frequency spectrum analysis of the noisy interferograms recorded during ECPL usage. Further, the results provide insights into the photopolymerization process at the micro-scale that were not previously evident.

2) The moving horizon exponentially weighted curve fitting method worked well in determining instantaneous frequencies in the interferograms. A study was performed to select the best parameter values for its use in typical ECPL experiments.

3) The proposed ICM method yielded promising results as a full-field sensor and as the basis for a global real-time feedback control system for the ECPL process.

More research effort is required in improving and implementing the method in real-time for the noisy physical ECPL system. One unique challenge for optical sensors and process control is the need for real-time parameters estimation, depending upon the speed of the process and the sampling time of the sensor [23]. Another challenge of in situ sensing and control is that the sensor measurement may have significant noise. Future work includes the following items.

- 1) To implement real-time measurement with the developed ICM method for the physical ECPL system.
- 2) To improve the ICM algorithms and reduce the effect of measurement noise.
- 3) To validate the ICM measurement system with noise handling strategies for real ECPL system.
- 4) To extend the current measurement of vertical height for measuring lateral dimensions, by calibrating an interferogram pixel's physical size that corresponds to the planar dimension of a cured part.

Acknowledgment

This material is based upon work supported by the National Science Foundation under Grant No. CMMI-1234561. Any opinions, findings, and conclusions or recommendations expressed in this publication are those of the authors and do not necessarily reflect the views of the National Science Foundation. All the related research is patent pending.

Reference

- [1] Jariwala, A.S., *Modeling And Process Planning For Exposure Controlled Projection Lithography*. Ph.D. thesis, Mechanical Engineering, Georgia Institute of Technology, Atlanta, USA, 2013.
- [2] Jariwala, A.S., R.E. Schwerzel, and D.W. Rosen, *Real-Time Interferometric Monitoring System For Exposure Controlled Projection Lithography*. Proceedings of the 22nd Solid Freeform Fabrication Symposium, 2011: p. 99-108.
- [3] Jones, H.H., et al., *Real-Time Selective Monitoring Of Exposure Controlled Projection Lithography*. Proceedings of the 24th Solid Freeform Fabrication Symposium, 2013: p. 55-65.
- [4] Creath, K., *Phase-measurement interferometry techniques*. Progress in optics, 1988. 26(26): p. 349-393.
- [5] Huntley, J.M. and H. Saldner, *Temporal phase-unwrapping algorithm for automated interferogram analysis*. Applied Optics, 1993. 32(17): p. 3047-3052.
- [6] Kaufmann, G.H. and G.E. Galizzi, *Phase measurement in temporal speckle pattern interferometry: comparison between the phase-shifting and the Fourier transform methods*. Applied Optics, 2002. 41(34): p. 7254-7263.
- [7] Colonna de Lega, X., *Processing of non-stationary interference patterns - adapted phase-shifting algorithms and wavelet analysis. Application to dynamic deformation measurements by*

- holographic and speckle interferometry*. Ph.D. dissertation, Swiss Federal Institute of Technology, 1997.
- [8] Gao, W., et al., *Real-time 2D parallel windowed Fourier transform for fringe pattern analysis using Graphics Processing Unit*. Optics Express, 2009. 17(25): p. 23147-23152.
- [9] Kemao, Q., H. Wang, and W. Gao, *Some Recent Developments of Windowed Fourier Transform for Fringe Pattern Analysis*. AIP Conference Proceedings, 2010. 1236(1): p. 106-111.
- [10] Jones, H.H., A.S. Jariwala, and D.W. Rosen, *Towards Real Time Control Of Exposure Controlled Projection Lithography*. Proceedings of International Symposium on Flexible Automation, 2014.
- [11] Takeda, M., H. Ina, and S. Kobayashi, *Fourier-transform method of fringe-pattern analysis for computer-based topography and interferometry*. Journal of the Optical Society of America, 1982. 72(1): p. 156-160.
- [12] Schwerzel, R.E., A.S. Jariwala, and D.W. Rosen, *A simple, inexpensive, real-time interferometric cure monitoring system for optically cured polymers*. Journal of Applied Polymer Science, 2013. 129(5): p. 2653-2662.
- [13] Federico, A. and G.H. Kaufmann, *Robust phase recovery in temporal speckle pattern interferometry using a 3D directional wavelet transform*. Optics letters, 2009. 34(15): p. 2336-2338.
- [14] Kai, L. and Q. Kemao, *Dynamic phase retrieval in temporal speckle pattern interferometry using least squares method and windowed Fourier filtering*. Optics Express, 2011. 19(19): p. 18058-18066.
- [15] Fu, Y., et al., *Kinematic and deformation parameter measurement by spatiotemporal analysis of an interferogram sequence*. Applied Optics, 2007. 46(36): p. 8645.
- [16] Breiland, W.G. and K.P. Killeen, *A virtual interface method for extracting growth rates and high temperature optical constants from thin semiconductor films using in situ normal incidence reflectance*. Journal of Applied Physics, 1995. 78(11): p. 6726-6736.
- [17] Meneses-Fabian, C. and U. Rivera-Ortega, *Phase-Shifting Interferometry by Amplitude Modulation*, in *Interferometry – Research and Applications in Science and Technology*, I. Padron, Editor. 2012, InTech. p. 171-194.
- [18] Tang, Y., *Stereolithography Cure Process Modeling*. PhD, School of Chemical & Biomolecular Engineering, Georgia Institute of Technology, Atlanta, 2005.
- [19] Stanković, L., et al., *Instantaneous frequency in time–frequency analysis: Enhanced concepts and performance of estimation algorithms*. Digital Signal Processing, 2014. 35: p. 1-13.
- [20] Grover, M.A. and R. Xiong, *A Modified Moving Horizon Estimator for In Situ Sensing of a Chemical Vapor Deposition Process*. Control Systems Technology, IEEE Transactions, 2009. 17(5): p. 1228 - 1235.
- [21] Soroush, M., *State and parameter estimations and their applications in process control*. Computers and Chemical Engineering, 1998. 23: p. 229-245.
- [22] Kurfess, T.R. and T.J. Hodgson, *Metrology, Sensors and Control*, in *Micromanufacturing*. 2007. p. 89-109.
- [23] Xiong, R. and M.A. Grover, *In Situ Optical Sensing and State Estimation for Control of Surface Processing*, in *Feedback Control of MEMS to Atoms*. 2012. p. 45-67.